

Breaking of Valley Degeneracy by Magnetic Field in Monolayer MoSe₂

David MacNeill,¹ Colin Heikes,¹ Kin Fai Mak,^{1,2} Zachary Anderson,¹ Andor Kormányos,³
Viktor Zólyomi,⁴ Jiwoong Park,^{5,2} and Daniel C. Ralph^{1,2}

¹*Department of Physics, Cornell University, Ithaca, New York 14853, USA*

²*Kavli Institute at Cornell, Cornell University, Ithaca, New York 14853, USA*

³*Department of Physics, University of Konstanz, D-78464 Konstanz, Germany*

⁴*Department of Physics, Lancaster University, Lancaster LA1 4YB, United Kingdom*

⁵*Department of Chemistry and Chemical Biology, Cornell University, Ithaca, New York 14853, USA*

(Received 1 July 2014; revised manuscript received 1 October 2014; published 22 January 2015)

Using polarization-resolved photoluminescence spectroscopy, we investigate the breaking of valley degeneracy by an out-of-plane magnetic field in back-gated monolayer MoSe₂ devices. We observe a linear splitting of -0.22 meV/T between luminescence peak energies in σ_+ and σ_- emission for both neutral and charged excitons. The optical selection rules of monolayer MoSe₂ couple the photon handedness to the exciton valley degree of freedom; so this splitting demonstrates valley degeneracy breaking. In addition, we find that the luminescence handedness can be controlled with a magnetic field to a degree that depends on the back-gate voltage. An applied magnetic field, therefore, provides effective strategies for control over the valley degree of freedom.

DOI: 10.1103/PhysRevLett.114.037401

PACS numbers: 78.67.-n, 78.20.Ls, 78.55.-m

Monolayer MoSe₂ and other monolayer transition metal dichalcogenides (TMDs) are a materials system with unique potential for controlling their valley degree of freedom [1–8]. Similar to graphene, the conduction and valence band show extrema (valleys) at the vertices of a hexagonal Brillouin zone; unlike graphene, MoSe₂ exhibits a nonzero optical gap of 1.66 eV [9,10]. This has allowed exploration of optoelectronic properties arising from the valley-dependent chirality of massive Dirac fermions predicted in the context of inversion symmetry broken graphene [11,12]. This chirality leads to optical selection rules coupling the exciton valley degree of freedom to photon handedness [2–7]. Using polarization-resolved spectroscopy, researchers have demonstrated valley-selective luminescence with near 100% fidelity [2,7]. Furthermore, the ability to pump valley-polarized carriers with circularly polarized light has been demonstrated through the valley Hall effect [8]. The chiral electronic states are also predicted to possess valley-contrasting orbital magnetic moments coupling valley pseudospin to magnetic field [11–17], which opens up the possibility for magnetic control over the valley degree of freedom [13,18].

Here, we demonstrate the use of magnetic fields to break valley degeneracy in a monolayer TMD. Specifically, we report polarization-resolved luminescence spectra for back-gated MoSe₂ devices at 4.2 K and in magnetic fields up to 6.7 T. We study the luminescence peak energies as a function of magnetic field, finding a linear splitting of -0.22 meV/T between peaks corresponding to light emission with different senses of circular polarization, σ_+ and σ_- . We interpret this as a Zeeman splitting due to valley-dependent magnetic moments. We also investigate the magnetic-field dependence of luminescence handedness,

finding that the emission becomes circularly polarized in a magnetic field even with unpolarized excitation and that the degree of this polarization can be increased to about 50% by gating the sample. This suggests that electric fields can facilitate the generation of valley-population imbalance in samples where valley degeneracy has been broken by a magnetic field. Our results demonstrate a recently proposed [18] strategy for generating valley populations and could lead to new approaches for controlling the valley degree of freedom in monolayer TMDs.

Our device geometry and measurement apparatus are shown in Figs. 1(a) and 1(b). All measurements were taken using a scanning confocal microscope integrated with a 7 T superconducting magnet dewar, with light coupled in and out of the system via a polarization-maintaining optical fiber (similar designs were reported in Refs. [19,20]). The light is focused into a roughly 1 μm diameter spot using a pair of aspheric lenses, and the sample is scanned using piezo-driven nanopositioners (from attocube). The sample, positioners, and optical components are placed in a vacuum cryostat which is then evacuated and lowered into a helium bath containing a superconducting magnet; helium exchange gas is added to ensure thermalization of the sample at 4.2 K. For the data in the main text, the excitation power was between 10 and 60 μW .

To enable polarization-resolved spectroscopy, a zero-order quartz $\lambda/4$ plate is placed between the aspheric lenses oriented at 45° to the fiber axes; this couples σ_+ and σ_- emission into orthogonal polarization modes of the fiber. The light exiting the fiber is directed through a rotatable polarizer, which selects one fiber mode for spectral analysis by a spectrometer with a thermoelectrically-cooled CCD. We can also create a circularly polarized excitation by

coupling linearly polarized light into one of the two fiber polarization modes, or create equal intensity excitation in σ_+ and σ_- polarization by coupling in light polarized at 45° to the fiber axes. We excite luminescence with light from a 1.89 eV laser diode, which is 230 meV blueshifted from the A exciton transition, and as a result, we see little dependence of the emission polarization on excitation polarization (see the Supplemental Material, Sec. 1 [21]). The conclusions discussed below are independent of excitation polarization.

To fabricate our samples, we exfoliate bulk MoSe_2 crystals (grown by direct vapor transport) onto 300 nm silicon oxide on silicon then use electron-beam lithography to define a single 0.5 nm Ti and 75 nm Au contact, allowing the use of the silicon substrate as a back gate. All data shown in the main text were taken from devices $D1$ and $D2$ pictured in Fig. 1(c). Figure 1(d) shows the $B = 0$ luminescence spectra of $D2$ at $-30, 0, 10,$ and 50 V. The peaks at 1.66 and 1.63 eV correspond to the neutral and charged A exciton, respectively, with a charged exciton (trion) binding energy of 30 meV [9]. As the back-gate voltage is increased, the exciton luminescence decreases and the trion luminescence increases, showing that our samples are intrinsically n type and that the 1.63 eV peak corresponds to negatively charged trion luminescence.

Figure 2(a) compares polarization-resolved spectra taken for $D1$ in out-of-plane magnetic fields of 0, 6.7, and -6.7 T and with the back gate grounded. For these data, we excite photoluminescence using equal intensity excitation in σ_+ and σ_- polarization. At zero field, we find no significant dependence of the peak energies or intensities on emission handedness. In comparison, the spectra taken at 6.7 T

show splitting between the σ_+ and σ_- emission peaks of about -1.5 meV for both the exciton and trion. The luminescence is also σ_+ polarized: the trion peak has $P_{\text{trion}} = (I_+ - I_-)/(I_+ + I_-) = 14\%$, where I_{\pm} is the peak intensity of the trion found with σ_{\pm} detection. For the exciton, we measure $P_{\text{exciton}} = 9\%$. The luminescence polarization changes sign with reversal of the magnetic field but not with excitation polarization, showing that it arises from magnetically induced changes in the exciton and trion populations. Figure 2(b) depicts the schematic band structure of a MoSe_2 monolayer, illustrating the direct band gaps at the K_+ and K_- points, with arrows indicating the allowed A exciton transitions for σ_{\pm} light. Since the emission handedness is coupled to the exciton valley degree of freedom, the peak splitting and polarization we observe indicate valley degeneracy breaking.

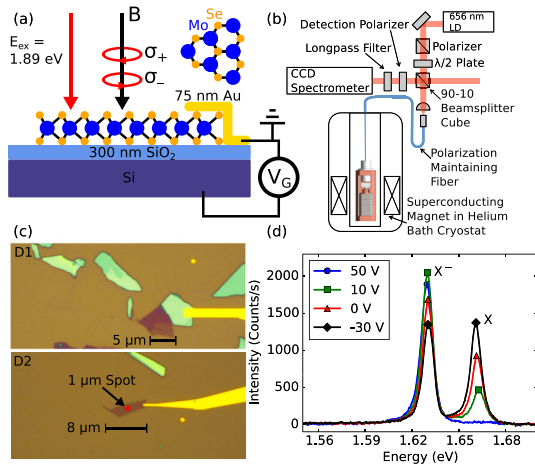


FIG. 1 (color online). (a) Experimental geometry showing back-gated monolayer MoSe_2 devices in out-of-plane magnetic fields. Luminescence is excited with light from a 1.89 eV laser diode and collected separately for σ_+ and σ_- polarization in the Faraday geometry. (b) Schematic of the fiber-coupled optical cryostat used in the experiment. (c) Optical micrographs of devices $D1$ and $D2$. (d) Luminescence spectra of $D2$ taken at 0 T and 4.2 K with $-30, 0, 10,$ and 50 V back-gate voltage.

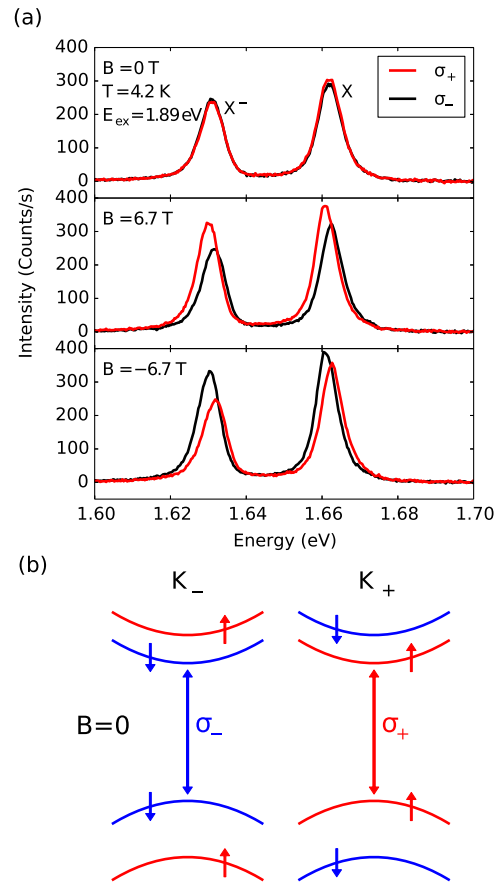


FIG. 2 (color online). (a) Polarization-resolved luminescence spectra from monolayer MoSe_2 ($D1$) at 4.2 K for σ_+ and σ_- detection, as excited using unpolarized light at 1.89 eV. From top to bottom, the panels show spectra taken with 0, 6.7, and -6.7 T out-of-plane magnetic fields. Both the polarization and splitting change sign upon reversing the field. (b) Schematic band structure of MoSe_2 near the K_+ and K_- points in the absence of a magnetic field, showing the optical selection rules for the A exciton transition studied in this experiment. Within each valley, spin degeneracy is broken at $B = 0$ due to spin-orbit coupling [9,10,13,40,41]. The arrows denote spin angular momentum up and down for the occupied states.

Figure 3(a) shows the valley splitting of the exciton and trion peaks, defined as the difference between peak energies found with σ_+ and σ_- detection, versus the magnetic field. For each data point, the peak positions were extracted via fits to a phenomenological asymmetric Voigt line shape (see the Supplemental Material, Sec. 2 [21]). The error bars come primarily from the CCD pixel size (about 0.15 nm per pixel). For both the exciton and trion peaks, the valley splitting shows a linear magnetic-field dependence with a slope of -0.22 ± 0.01 meV/T. Similar results were found on three separate samples; data from other samples are given in the Supplemental Material, Sec. 3 [21].

Valley splitting in a magnetic field arises from the intrinsic chirality of Bloch electrons at the K_+ and K_- points. States at the two valley edges are Kramers doublets related by time-reversal symmetry, so that their degeneracy can be broken by breaking time-reversal symmetry. Bloch electrons in a given band carry spin and orbital magnetic moments which change sign between valleys [11–13,42]. Figure 3(b) schematically shows the energy shifts arising from Zeeman coupling between these moments and the magnetic field; there, we define $2E_Z^{c(v)}$ as the magnetic-field-induced energy difference between the K_+ and K_- valley at the conduction (valence) band edge. Magnetoluminescence spectroscopy probes

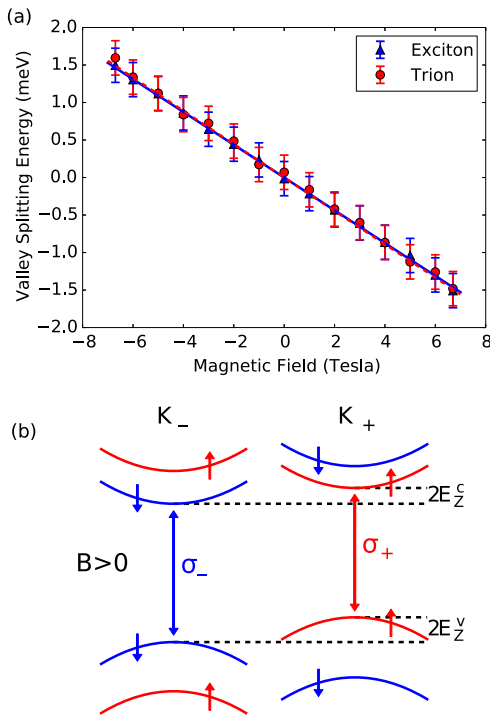


FIG. 3 (color online). (a) Difference of peak energies found for σ_+ and σ_- detection plotted versus the magnetic field for D1. Both the exciton (blue triangles) and trion (red circles) show splitting of -0.22 ± 0.01 meV/T found via a linear fit. The fits are plotted as blue solid and red dashed lines for the exciton and trion, respectively. (b) The schematic band structure of MoSe₂ in a magnetic field showing the Zeeman energy $E_Z^{c(v)}$ for the conduction (valence) band. The exciton Zeeman splitting is $2(E_Z^c - E_Z^v)$.

only the exciton Zeeman energy, which is the difference between the conduction and valence band Zeeman energies. In this difference, the contributions from spin magnetic moments are expected to cancel, leaving only the contributions from orbital magnetic moments.

The measured sign and magnitude of the valley splitting can be understood within a tight-binding picture [43,44]. In the K_τ valley (letting $\tau = \pm 1$ be the valley quantum number), the valence band arises from hybridization of $d_{x^2-y^2} + \tau id_{xy}$ orbitals with angular momentum $l_z = 2\tau\hbar$, while the conduction band arises from hybridization of d_{z^2} orbitals with $l_z = 0$ [1,6,41,45]. In the tight-binding limit, we, therefore, expect a contribution to the exciton Zeeman energy of $2(E_{Z,a}^c - E_{Z,a}^v) = -4\mu_B B$ from atomic-scale magnetic moments. The phase winding of Bloch states on the intercellular scale can also add to the orbital magnetic moment [11,42–44,46]. For example, in the two-band tight-binding model (the massive Dirac fermion model), the intercellular magnetic moment is the same for the conduction and valence bands with value $-\tau\mu_B(m_e/m_{\text{eff}})$, where m_e is the free-electron mass, and m_{eff} is the electron-hole symmetric carrier effective mass [11,12]. Including the spin magnetic moments, this gives a total Zeeman splitting of $2E_Z^c = 2\mu_B + 2\mu_B(m_e/m_{\text{eff}})$ for the conduction band and $2E_Z^v = 2\mu_B B + 4\mu_B B + 2\mu_B B(m_e/m_{\text{eff}})$ for the valence band, and as a result, $2(E_Z^c - E_Z^v) = -4\mu_B B$ (i.e., there is no net intercellular contribution). In more general hopping models, the conduction and valence bands can have different intercellular moments giving a net contribution to the exciton magnetic moment [16,40,43,44].

To compare our measurements with theory, we define the exciton valley g factor $g_{\text{ex}}^{\text{vl}}$ as

$$g_{\text{ex}}^{\text{vl}} = \frac{2(E_+ - E_-)}{\mu_B B} = \frac{2(E_Z^c - E_Z^v)}{\mu_B B}, \quad (1)$$

where E_\pm is the measured exciton peak energy in the σ_\pm detection. Our exciton valley splitting measurements correspond to $g_{\text{ex}}^{\text{vl}} = -3.8 \pm 0.2$, consistent with the value of $g_{\text{ex}}^{\text{vl}} = -4$ expected from the d -orbital contribution to the exciton magnetic moment. Any deviation of $g_{\text{ex}}^{\text{vl}}$ from -4 theoretically corresponds to the intercellular contribution to the g factor. Our results, therefore, suggest that the intercellular contribution to $g_{\text{ex}}^{\text{vl}}$ is small in the case of MoSe₂. We also expect the trion to have approximately the same splitting as the exciton, evinced by considering the trion as an exciton bound to an additional electron. While the additional electron contributes to the trion magnetic moment, it contributes equally to the final state moment after recombination, leaving the transition energy unaffected (as discussed in more detail in the Supplemental Material, Sec. 4 [21]). This is consistent with the experimental results of Fig. 3(a) for zero applied gate voltage.

We also attempted to calculate the valley g factor using the multiband $\mathbf{k} \cdot \mathbf{p}$ theory of Ref. [13], since this theory should include the intercellular and atomic contributions in a unified way [46]. The need to discuss these terms separately

is an artifact of the lattice models discussed above. The calculation is detailed in Sec. 5 of the Supplemental Material [21] and gives a value for $g_{\text{ex}}^{\text{vl}}$ similar in magnitude to our experimental results, but with the opposite sign (see the Supplemental Material, Sec. 6 for our experimental determination of the sign [21]). Therefore, further theoretical work is required to understand the exciton valley splitting within the context of $\mathbf{k} \cdot \mathbf{p}$ theory calculations.

We find that the trion valley splitting and the resulting luminescence polarization both show a surprising dependence on an applied back-gate voltage. Polarization-resolved spectra taken with -20 and 51 V applied to the substrate are shown in Fig. 4(a) for device *D2*. Our samples show significant hysteresis assumed to arise from photoionization of trap states [47], and the data in this panel are taken from a downward sweep. Figure 4(b) shows the trion splitting versus magnetic field for two different gate voltages on a downward sweep, finding -0.29 ± 0.02 meV/T at 40 V and -0.23 ± 0.02 meV/T at 0 V. This gate-voltage dependence of the trion splitting could arise from carrier-density dependence of the band Zeeman energies [11,16], a hot luminescence effect as discussed in Sec. 4 of the Supplemental Material [21] or other effects resulting from changes in the trion or final state wave functions upon increasing the Fermi level [48]. The gate dependence of trion valley splitting has implications for future magneto-optical studies of TMDs, as the intrinsic doping level may vary between samples causing a dispersion of measurement results.

The degree of trion polarization as a function of gate voltage is shown in Fig. 4(c). In this data set, we find a trion polarization that increases from 18% near zero back-gate voltage to over 50% near 40 V. The luminescence

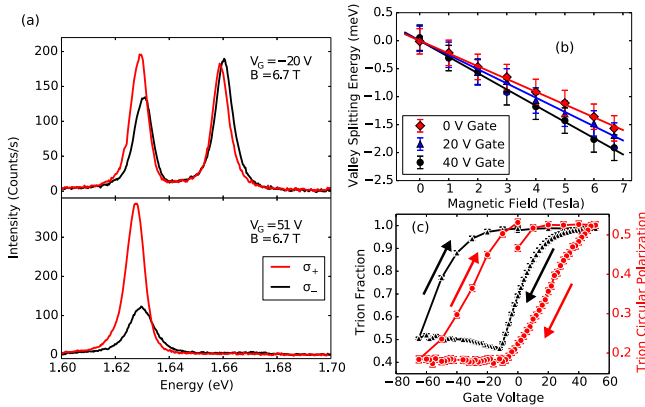


FIG. 4 (color online). (a) Polarization-resolved luminescence spectra from *D2* at 4.2 K and 6.7 T for σ_+ and σ_- detection, excited with σ_- light at 1.89 eV. From top to bottom, the panels show spectra taken with -20 and 51 V gate voltage applied to the substrate. (b) Trion valley splitting versus the magnetic field for selected gate voltages, showing a decrease in slope with gate voltage. (c) Circular polarization of the trion peak $(I_+ - I_-)/(I_+ + I_-)$ versus gate voltage at 6.7 T (red circles), showing an increase to over 50% as gate voltage is increased. For comparison, we also plot the trion fraction $I_{\text{trion}}/(I_{\text{trion}} + I_{\text{exciton}})$ (black triangles).

polarization in the n -type regime is related to the populations of different trion species via $P_{\text{trion}} = (n_+ - n_-)/(n_+ + n_-)$, where n_{\pm} is the density of negatively charged trions with their hole in valley K_{\pm} (i.e., those which emit σ_{\pm} -polarized light upon recombination, which we refer to as K_{\pm} valley trions). The sign of P_{trion} is found to be independent of the excitation polarization and instead follows the sign of the magnetic field, and we, therefore, interpret the magnetic-field dependence of the trion polarization as arising from partial relaxation of trions into their lowest energy spin-valley configuration (qualitatively consistent with the dependence of trion polarization on excitation power, see the Supplemental Material, Sec. 7 [21]). This relaxation is expected to be incomplete, as the intervalley scattering time is longer than the recombination time [2]. In Sec. 4 of the Supplemental Material, we calculate the trion polarization within a simple rate-equation model and show that the observed P_{trion} implies a ratio of the recombination time to the intervalley scattering time of ~ 0.2 at low carrier density [21]. This is about an order of magnitude larger than the value found in time-resolved measurements for WSe₂ at zero magnetic field [49]; however, the time-resolved measurements used resonant excitation which is expected to lead to reduced intervalley scattering compared to the off-resonant excitation we use. Trions can scatter between valleys via spin-flip intervalley scattering of their hole, and if this is the dominant scattering mechanism, our results imply that the hole intervalley scattering rate increases monotonically with carrier density. This is consistent with the Bir-Aronov-Pikus mechanism for intervalley scattering of holes via their exchange interaction with the conduction electrons [2,50]. The data in Fig. 4(c) were taken with σ_- excitation, but similar results were found using unpolarized excitation (see Sec. 3 of the Supplemental Material [21]).

In summary, we have presented measurements of polarization-resolved luminescence spectra for MoSe₂ at 4.2 K in magnetic fields up to 6.7 T, demonstrating valley degeneracy breaking. We have measured a splitting of -0.22 ± 0.01 meV/T between exciton peaks in σ_+ - and σ_- -polarized emission spectra. This value is consistent with a simple tight-binding picture of the MoSe₂ band structure. We have also observed gate dependence of the trion valley splitting and polarization. Even with off-resonant unpolarized excitation, we were able to achieve a trion circular polarization of about 50% by gating the sample in a 6.7 T magnetic field. The application of magnetic and electric fields can, therefore, provide an effective strategy for manipulating the valley degree of freedom in monolayer TMDs.

Similar work on WSe₂ has recently been posted by the Washington group [44] and the ETH Zurich group [43].

We thank Kathryn McGill and Joshua Kevek for growth of the bulk MoSe₂ crystal used for this work. We also thank Guido Burkard, Péter Rakytá, Alexander Högele, and

Ermin Malic for helpful discussions. This research was supported in part by the NSF (Grant No. DMR-1010768) and the Kavli Institute at Cornell for Nanoscale Science. We also made use of the Cornell Center for Materials Research Shared Facilities which are supported through the NSF Materials Research Science and Engineering Center program (Grant No. DMR-1120296). Device fabrication was performed at the Cornell NanoScale Facility, a member of the National Nanotechnology Infrastructure Network, which is supported by the National Science Foundation (Grant No. ECCS-0335765). D. M. acknowledges support from a Natural Sciences and Engineering Research Council of Canada Postgraduate Scholarship.

-
- [1] D. Xiao, G.-B. Liu, W. Feng, X. Xu, and W. Yao, *Phys. Rev. Lett.* **108**, 196802 (2012).
- [2] K. F. Mak, K. He, J. Shan, and T. F. Heinz, *Nat. Nanotechnol.* **7**, 494 (2012).
- [3] A. M. Jones, H. Yu, N. J. Ghimire, S. Wu, G. Aivazian, J. S. Ross, B. Zhao, J. Yan, D. G. Mandrus, D. Xiao, W. Yao, and X. Xu, *Nat. Nanotechnol.* **8**, 634 (2013).
- [4] G. Kioseoglou, A. T. Hanbicki, M. Currie, A. L. Friedman, D. Gunlycke, and B. T. Jonker, *Appl. Phys. Lett.* **101**, 221907 (2012).
- [5] H. Zeng, J. Dai, W. Yao, D. Xiao, and X. Cui, *Nat. Nanotechnol.* **7**, 490 (2012).
- [6] T. Cao, G. Wang, W. Han, H. Ye, C. Zhu, J. Shi, Q. Niu, P. Tan, E. Wang, B. Liu, and J. Feng, *Nat. Commun.* **3**, 887 (2012).
- [7] G. Sallen, L. Bouet, X. Marie, G. Wang, C. R. Zhu, W. P. Han, Y. Lu, P. H. Tan, T. Amand, B. L. Liu, and B. Urbaszek, *Phys. Rev. B* **86**, 081301 (2012).
- [8] K. F. Mak, K. L. McGill, J. Park, and P. L. McEuen, *Science* **344**, 1489 (2014).
- [9] J. S. Ross, S. Wu, H. Yu, N. J. Ghimire, A. M. Jones, G. Aivazian, J. Yan, D. G. Mandrus, D. Xiao, W. Yao, and X. Xu, *Nat. Commun.* **4**, 1474 (2013).
- [10] Y. Zhang, T.-R. Chang, B. Zhou, Y.-T. Cui, H. Yan, Z. Liu, F. Schmitt, J. Lee, R. Moore, Y. Chen, H. Lin, H.-T. Jeng, S.-K. Mo, Z. Hussain, A. Bansil, and Z.-X. Shen, *Nat. Nanotechnol.* **9**, 111 (2013).
- [11] D. Xiao, W. Yao, and Q. Niu, *Phys. Rev. Lett.* **99**, 236809 (2007).
- [12] W. Yao, D. Xiao, and Q. Niu, *Phys. Rev. B* **77**, 235406 (2008).
- [13] A. Kormányos, V. Zólyomi, N. D. Drummond, and G. Burkard, *Phys. Rev. X* **4**, 011034 (2014).
- [14] X. Li, F. Zhang, and Q. Niu, *Phys. Rev. Lett.* **110**, 066803 (2013).
- [15] R.-L. Chu, X. Li, S. Wu, Q. Niu, W. Yao, X. Xu, and C. Zhang, *Phys. Rev. B* **90**, 045427 (2014).
- [16] H. Rostami, A. G. Moghaddam, and R. Asgari, *Phys. Rev. B* **88**, 085440 (2013).
- [17] Y.-H. Ho, Y.-H. Wang, and H.-Y. Chen, *Phys. Rev. B* **89**, 155316 (2014).
- [18] T. Cai, S. A. Yang, X. Li, F. Zhang, J. Shi, W. Yao, and Q. Niu, *Phys. Rev. B* **88**, 115140 (2013).
- [19] A. Högele, S. Seidl, M. Kroner, K. Karrai, C. Schulhauser, O. Sqalli, J. Scrimgeour, and R. J. Warburton, *Rev. Sci. Instrum.* **79**, 023709 (2008).
- [20] M. Sladkov, M. Bakker, A. Chaubal, D. Reuter, A. Wieck, and C. van der Wal, *Rev. Sci. Instrum.* **82**, 043105 (2011).
- [21] See Supplemental Material at <http://link.aps.org/supplemental/10.1103/PhysRevLett.114.037401>, which includes Refs. [22–39], for additional details of the data analysis, experimental methods, and theoretical calculations of the valley splitting and polarization.
- [22] J. Ma and Y.-S. Li, *Appl. Opt.* **35**, 2527 (1996).
- [23] H. Yu, G.-B. Liu, P. Gong, X. Xu, and W. Yao, *Nat. Commun.* **5**, 3876 (2014).
- [24] C. R. L. P. N. Jeukens, P. C. M. Christianen, J. C. Maan, D. R. Yakovlev, W. Ossau, V. P. Kochereshko, T. Wojtowicz, G. Karczewski, and J. Kossut, *Phys. Rev. B* **66**, 235318 (2002).
- [25] J. M. Luttinger, *Phys. Rev.* **102**, 1030 (1956).
- [26] L. M. Roth, *Phys. Rev.* **118**, 1534 (1960).
- [27] S. Wu, J. S. Ross, G.-B. Liu, G. Aivazian, A. Jones, Z. Fei, W. Zhu, D. Xiao, W. Yao, D. Cobden, and X. Xu, *Nat. Phys.* **9**, 149 (2013).
- [28] A. Kormányos, V. Zólyomi, M. Gmitra, N. D. Drummond, J. Fabian, V. Fal'ko, and G. Burkard, [arXiv:1410.6666](https://arxiv.org/abs/1410.6666).
- [29] A. Ramasubramaniam, *Phys. Rev. B* **86**, 115409 (2012).
- [30] R. S. Knox, *Theory of Excitons* (Academic Press, New York, 1963).
- [31] N. A. Gippius, A. L. Yablonskii, A. B. Dzyubenko, S. G. Tikhodeev, L. V. Kulik, V. D. Kulakovskii, and A. Forchel, *J. Appl. Phys.* **83**, 5410 (1998).
- [32] G. Berghäuser and E. Malic, *Phys. Rev. B* **89**, 125309 (2014).
- [33] T. C. Berkelbach, M. S. Hybertsen, and D. R. Reichman, *Phys. Rev. B* **88**, 045318 (2013).
- [34] M. Sugawara, N. Okazaki, T. Fujii, and S. Yamazaki, *Phys. Rev. B* **48**, 8848 (1993).
- [35] H. Q. Hou, W. Staguhn, S. Takeyama, N. Miura, Y. Segawa, Y. Aoyagi, and S. Namba, *Phys. Rev. B* **43**, 4152 (1991).
- [36] D. C. Rogers, J. Singleton, R. J. Nicholas, C. T. Foxon, and K. Woodbridge, *Phys. Rev. B* **34**, 4002 (1986).
- [37] A. V. Malyavkin, *Solid State Commun.* **39**, 1315 (1981).
- [38] E. Molva and L. S. Dang, *Phys. Rev. B* **27**, 6222 (1983).
- [39] E. Molva and L. S. Dang, *Phys. Rev. B* **32**, 1156 (1985).
- [40] G.-B. Liu, W.-Y. Shan, Y. Yao, W. Yao, and D. Xiao, *Phys. Rev. B* **88**, 085433 (2013).
- [41] K. Kośmider, J. W. González, and J. Fernández-Rossier, *Phys. Rev. B* **88**, 245436 (2013).
- [42] M.-C. Chang and Q. Niu, *J. Phys. Condens. Matter* **20**, 193202 (2008).
- [43] A. Srivastava, M. Sidler, A. V. Allain, D. S. Lembke, A. Kis, and A. Imamoglu, [arXiv:1407.2624](https://arxiv.org/abs/1407.2624).
- [44] G. Aivazian, Z. Gong, A. M. Jones, R.-L. Chu, J. Yan, D. G. Mandrus, C. Zhang, D. Cobden, W. Yao, and X. Xu, [arXiv:1407.2645](https://arxiv.org/abs/1407.2645).
- [45] Z. Y. Zhu, Y. C. Cheng, and U. Schwingenschlögl, *Phys. Rev. B* **84**, 153402 (2011).
- [46] Y. Yafet, *Solid State Phys.* **14**, 1 (1963).
- [47] A. A. Mitioglu, P. Plochocka, J. N. Jadczak, W. Escoffier, G. L. J. A. Rikken, L. Kulyuk, and D. K. Maude, *Phys. Rev. B* **88**, 245403 (2013).
- [48] C. Zhang, H. Wang, W. Chan, C. Manolatou, and F. Rana, *Phys. Rev. B* **89**, 205436 (2014).
- [49] G. Wang, L. Bouet, D. Lagarde, M. Vidal, A. Balocchi, T. Amand, X. Marie, and B. Urbaszek, *Phys. Rev. B* **90**, 075413 (2014).
- [50] G. L. Bir, A. G. Aronov, and G. E. Pikus, *Zh. Eksp. Teor. Fiz.* **69**, 1382 (1976) [*Sov. Phys. JETP* **42**, 705 (1976)].

Supplement to “Breaking of Valley Degeneracy by Magnetic Field in Monolayer MoSe₂”

David MacNeill,¹ Colin Heikes,¹ Kin Fai Mak,^{1,2} Zachary Anderson,¹ Andor Kormányos,³ Viktor Zólyomi,⁴ Jiwoong Park,^{5,2} and Daniel C. Ralph^{1,2}

¹*Department of Physics, Cornell University, Ithaca, NY 14853, USA*

²*Kavli Institute at Cornell, Cornell University, Ithaca, NY 14853, USA*

³*Department of Physics, University of Konstanz, D-78464 Konstanz, Germany*

⁴*Department of Physics, Lancaster University, Lancaster LA1 4YB, United Kingdom*

⁵*Department of Chemistry and Chemical Biology, Cornell University, Ithaca, NY 14853, USA*

(Dated: December 18, 2014)

1. DEPENDENCE OF LUMINESCENCE HANDEDNESS ON EXCITATION HANDEDNESS

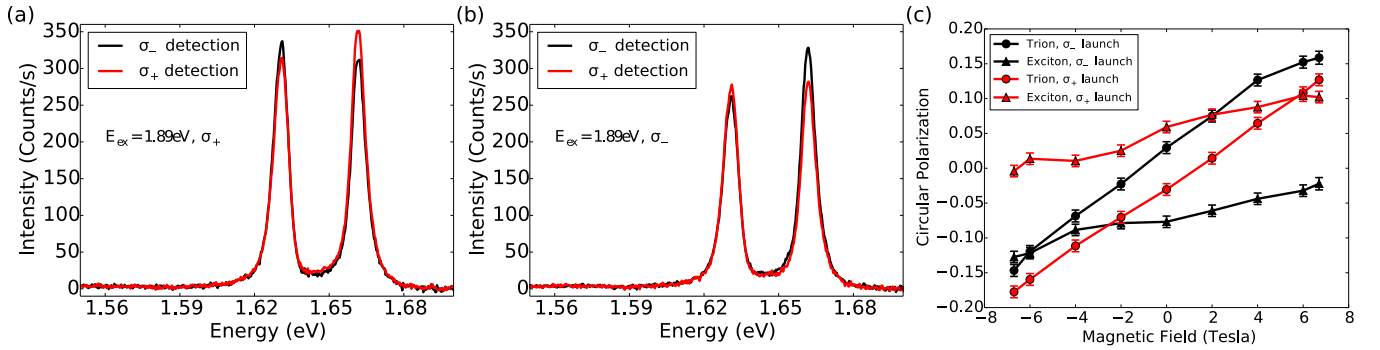


FIG. 1. (a) Polarization-resolved spectra from D1 taken at zero magnetic field and with σ_+ excitation, showing σ_+ polarization of exciton luminescence. (b) Polarization-resolved spectra from D1 taken at zero magnetic field and with σ_- excitation. (c) Luminescence polarization versus magnetic field with σ_+ (red) and σ_- (black) excitation for excitons (triangles) and trions (circles).

Figures 1a and 1b show polarization-resolved luminescence spectra for D1 at $T = 4.2$ K and $B = 0$ T taken with σ_+ and σ_- polarized excitation respectively. We observe some preservation of the incident polarization even with our 1.89 eV excitation. We find $P_{\text{exciton}} = \frac{I_+ - I_-}{I_+ + I_-} = 6\%$ for σ_+ excitation and $P_{\text{exciton}} = -8\%$ for σ_- excitation indicating 7% average co-polarization of exciton luminescence with the excitation laser. On the other hand, we see counter polarization of 3% for the trion luminescence. We also studied the dependence of the field-induced polarization on excitation handedness: as shown in Fig. 1c switching the excitation polarization seemingly adds a constant offset. The small polarization preservation we observe is consistent with studies of polarization preservation in MoS₂ using off-resonant excitation [1, 2].

2. BACKGROUND SUBTRACTION AND FITTING

Raman scattering of the excitation laser in the fiber presents a significant background in our experiment, as has been reported elsewhere [3, 4]. A spectrum of fiber Raman excited with 705 nm light is plotted in Fig. 2a, showing fused silica Raman peaks [4]. Since we excite with 656 nm light we encounter only the tail of this signal during measurements of MoSe₂ luminescence. To account for this background, we take additional spectra with the excitation laser spot on silicon; the background spectrum is then subtracted from the signal after carrying out a dark-count subtraction on both spectra. This is shown in Figs. 2b and 2c. In practice, we rescale the background to match the signal spectrum away from the luminescence peaks, to account for laser-power fluctuations and to allow a single background spectrum to be used multiple times. In Figs. 2b and 2c we have used the data without rescaling to prove that fiber Raman entirely accounts for the background.

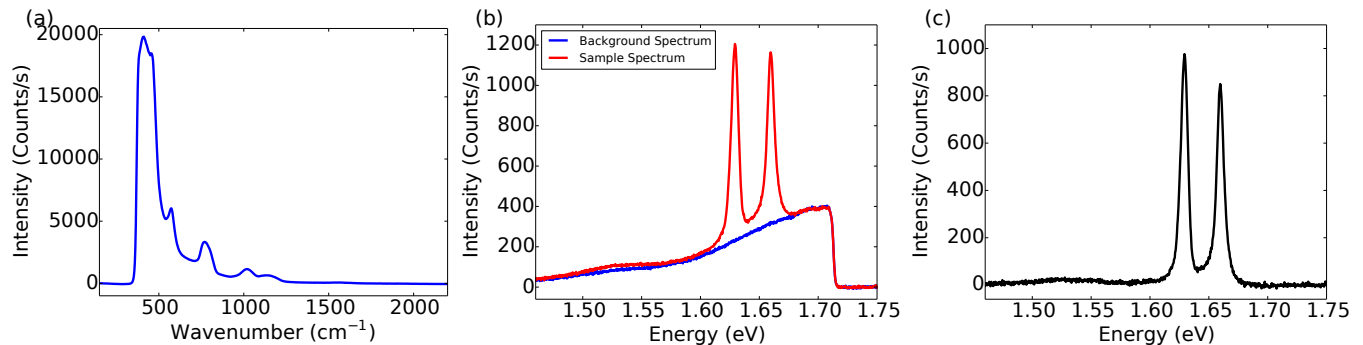


FIG. 2. (a) Fiber background spectrum excited with 705 nm laser diode, showing fused silica Raman peaks. (b) Comparison of spectra taken with 656 nm excitation laser on the sample (red) and on a nearby region of bare substrate (blue). (c) The result of subtracting the two curves in (b).

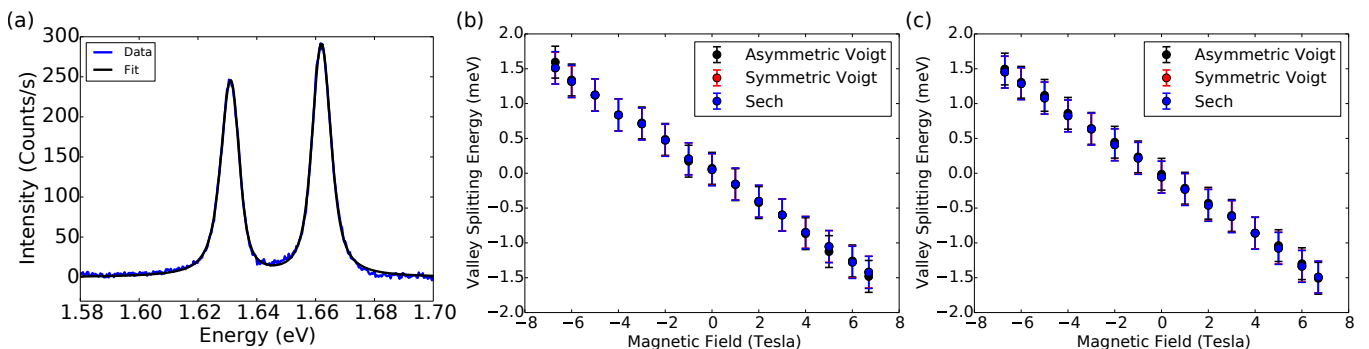


FIG. 3. (a) Comparison of sample luminescence spectrum (blue) and fit used to locate peak energy (black). The spectrum is fit to the sum of two asymmetric Voigt profiles, with $\chi^2 \approx 3$ (b) Trion valley splitting as extracted with fits to asymmetric Voigt (black), symmetric Voigt (red), and hyperbolic secant (blue). (c) Exciton valley splitting as extracted with fits to asymmetric Voigt (black), symmetric Voigt (red), and hyperbolic secant (blue). Valley splittings from asymmetric Voigt fits are presented in Fig. 3 of the main text.

In the main text we report values for the peak polarization and energy as a function of magnetic field and gating. As described there, we use fits to an asymmetric Voigt profile to extract the peak properties. The Voigt function is defined as:

$$\frac{1}{\sigma\sqrt{2\pi}} \operatorname{Re} \left\{ \exp \left[- \left(\frac{\delta\omega + i\gamma}{\sqrt{2}\sigma} \right)^2 \right] \operatorname{erfc} \left[-i \left(\frac{\delta\omega + i\gamma}{\sqrt{2}\sigma} \right) \right] \right\}, \quad (1)$$

where $\delta\omega$ is the detuning and γ and σ are fit parameters characterizing the peak width. As written, the function describes the convolution of a Lorentzian with width γ and a Gaussian with width σ ; to make the line shape asymmetric we allow γ to take different values for positive and negative detuning. A typical spectrum with fit is plotted in Fig. 3a; in this case the χ^2 was about 3. We also tried fitting to other functions, such as a hyperbolic secant and a symmetric Voigt profile. There was no difference in the valley splitting within our error bars. A comparison of splitting energies between symmetric Voigt, hyperbolic secant and asymmetric Voigt is shown in Figs. 3b and 3c.

3. COMPARISON OF DATA FROM MULTIPLE DEVICES

We measured the valley splitting versus magnetic field with the back-gate grounded for three different devices. All data were taken at 4.2 K and with 1.89 eV excitation. Valley splitting data not shown in the main text are given in Fig. 4; D1 and D2 are defined in the main text, and the additional device is called D3. For D3, we took data at two different positions on the flake. We have also provided Table I showing the slopes extracted from linear fits to

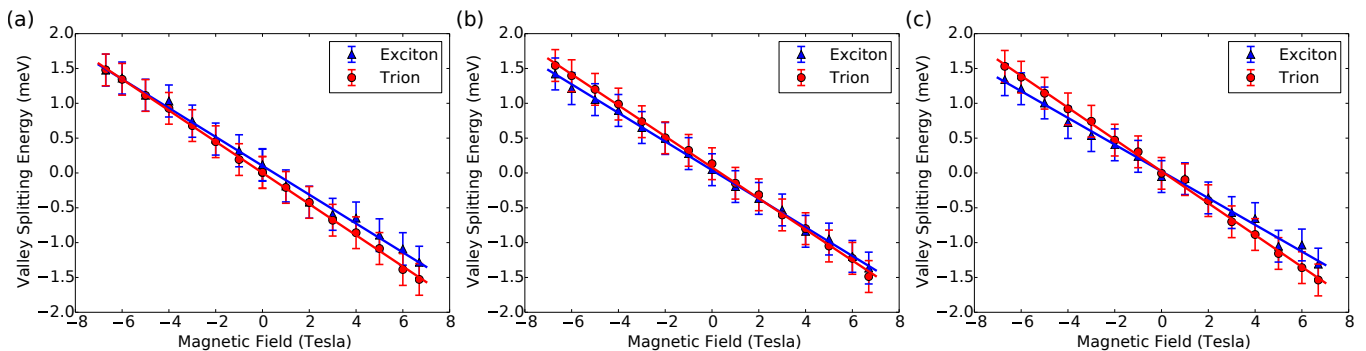


FIG. 4. (a) Valley splitting data for D1, as defined in the main text. (b) Valley splitting data taken near the center of D3. (c) Valley splitting data taken near one edge of D3.

this data. The standard deviation across datasets was $0.004 \frac{\text{meV}}{\text{T}}$ for the trion splitting and $0.01 \frac{\text{meV}}{\text{T}}$ for the exciton splitting. For one of the locations on D3, there was a significant discrepancy between the exciton and trion splitting.

Sample	Exciton Splitting ($\frac{\text{meV}}{\text{T}}$)	Trion Splitting ($\frac{\text{meV}}{\text{T}}$)
D1	-0.22	-0.22
D2	-0.21	-0.22
D3 location 1	-0.21	-0.22
D3 location 2	-0.19	-0.23

TABLE I. Valley splitting for multiple devices in $\frac{\text{meV}}{\text{T}}$, defined as the difference of luminescence peak energies between σ_+ and σ_- polarized light. The error for all values is $\pm 0.01 \frac{\text{meV}}{\text{T}}$.

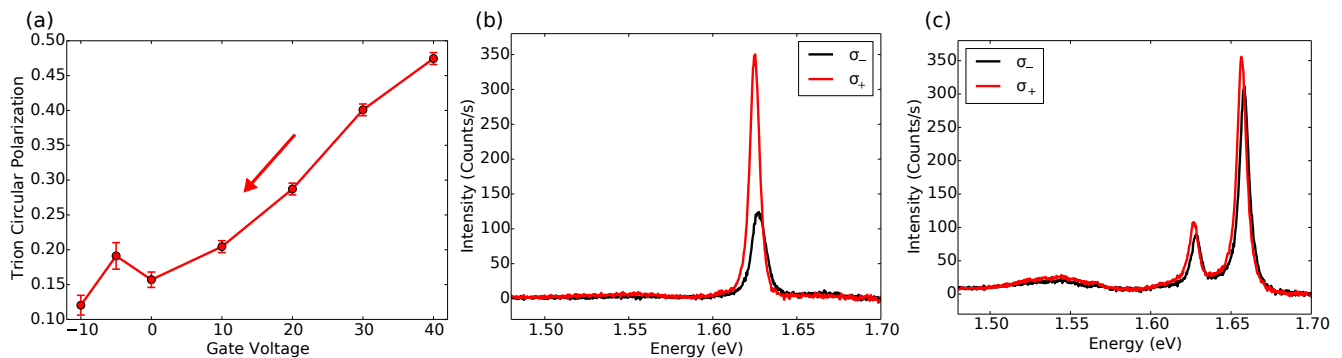


FIG. 5. (a) Trion peak polarization versus gate voltage at $B = 6.7 \text{ T}$ for D4 taken on a downward sweep and using $11 \mu\text{W}$ excitation with equal intensity in σ_+ and σ_- light (b) Polarization-resolved luminescence spectrum of D4 taken at 6.7 T magnetic field and 40 V back-gate voltage. (c) Polarization-resolved luminescence spectrum of D4 taken at 6.7 T magnetic field and -20 V back-gate voltage. The trion polarization is significantly reduced compared to the 40 V spectrum.

We also measured the gate dependence of valley splitting and polarization on two devices: D2 and another device not previously defined, D4. The gate dependence of luminescence from D4 is shown in Fig. 5. As shown in Fig. 5a, for D4 the trion polarization increases from about 10% to over 45% as the electron density is increased. For the data in Fig. 5 we used excitation light with equal intensity in σ_+ and σ_- polarization, and about $11 \mu\text{W}$ excitation power.

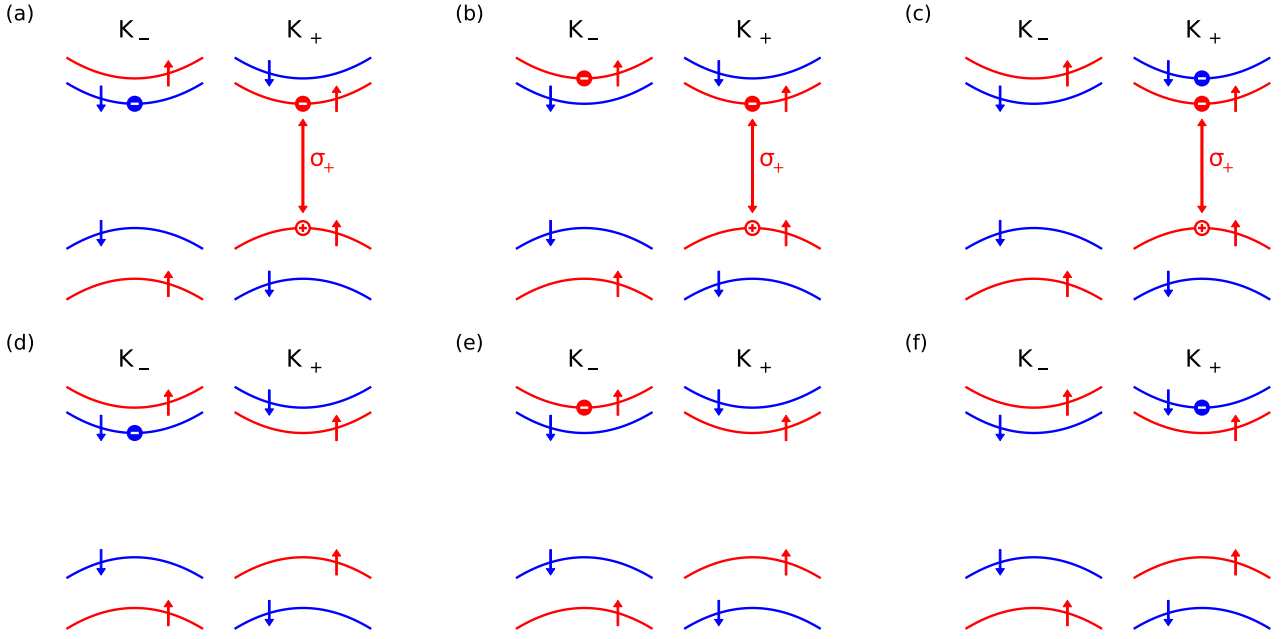


FIG. 6. Here we show the three possible trion spin-valley configurations which emit σ_+ polarized light on recombination (panels (a)-(c)) and the corresponding final states after recombination (panels (d)-(f)). In these schematic drawings, the full circles represent the two electrons in the trion, and the open circle represents the hole. We have arranged the panels so that the final state is below the initial state. The configurations shown here are the complete set of trion configurations emitting σ_+ light, but there are three more which emit σ_- light which are related to these via time-reversal symmetry. For the gate-voltage regime considered in our experiment, we expect that photoluminescence primarily arises from recombination of the trion species in panel (a) and its time-reversed partner.

4. FURTHER DISCUSSION OF THE TRION LUMINESCENCE AND ITS GATE VOLTAGE DEPENDENCE

Figure 6 shows the three possible negatively-charged trion spin-valley configurations which emit σ_+ polarization light on recombination (upper panels) and the corresponding final states after recombination (lower panels). These are the trion species defined as K_+ valley trions in the main text. There are also three more trion configurations not shown in Fig. 6 (the K_- valley trions) which are related to the configurations shown by time-reversal symmetry, and which emit σ_- light on recombination. In total there are then six trion configurations expected to have approximately the same binding energy, although the electron-hole exchange interaction is predicted to increase the energy of trions with parallel electron spins by about 6 meV [5]. Any trion configurations in which the two electrons have the same quantum numbers (spin and valley) have not been included in this accounting since they are not expected to be bound due to Pauli blocking. For MoSe₂ at low carrier density, only the lowest conduction bands will be occupied at 4.2 K since the conduction band spin-splitting is predicted to be about 20 meV [6–8]. As a result, the trion species in panel (a) is expected to be dominant at low carrier density. Based on Fig. 4d of the main text, we see that the conduction band edge for our samples is at approximately -12 V on a downsweep and therefore as an upper bound we gate into the conduction band by about $\frac{C\Delta V}{eA} / \frac{m_c}{\pi\hbar^2} \approx 20$ meV at our highest gate voltages (using $C \approx 1.2 \times 10^{-8}$ F/cm⁻¹ as the back-gate capacitance per unit area). The presence of trap states means this is probably an overestimate and we expect that the observed luminescence signal primarily arises from recombination of the panel (a) trion (and the time reversed version emitting σ_- light) at all gate voltages studied in this work.

In magnetic field, the total Zeeman energy of the trion can be approximated as the sum of the Zeeman energies of its constituent electrons and hole (the hole Zeeman energy being minus that of the relevant valence band). For example, the photon emitted when the trion in panel (a) recombines has energy: $E_{\text{initial}} - E_{\text{final}} = \epsilon_c + E_Z^c - \epsilon_v - E_Z^v + \epsilon_c - E_Z^c - E_B - (\epsilon_c - E_Z^c) = \epsilon_c - \epsilon_v - E_B + E_Z^c - E_Z^v = \hbar\omega + E_Z^c - E_Z^v$, where E_B is the sum of the exciton and trion binding energies (i.e. the total trion binding energy below the electronic band-gap), and $\hbar\omega$ is the trion emission energy for zero magnetic field. The trion valley splitting is then $2(E_Z^c - E_Z^v)$ and equal to the exciton valley

splitting. Similar calculations give the same results for the transitions shown in panels (b) and (c).

To estimate the gate dependence of the trion polarization we use a simple rate-equation model. In this model we assume that, for $B > 0$, the conversion rate of K_+ valley trions into K_- valley trions is suppressed by a Boltzmann factor of $e^{-2\beta E_Z^v}$ compared to the time-reversed process [9], where $\beta = \frac{1}{k_B T}$ with T the effective temperature of the trion population. The argument of the Boltzmann factor is determined by the energy barrier for switching from the trion species in panel a), with its hole in K_+ valley, to its time reversed partner with a hole in K_- valley: this energy is given by $E_{\text{initial}}(K_-) - E_{\text{initial}}(K_+) = 2E_Z^v$. We will also assume that, due to our off-resonant excitation, the formation rate Q of K_+ and K_- trions is roughly equal. The resulting rate equation is:

$$\begin{cases} \frac{dn_+}{dt} = Q - n_+/\tau_R + n_-/\tau_{v1} - n_+e^{-2\beta E_Z^v}/\tau_{v1} \\ \frac{dn_-}{dt} = Q - n_-/\tau_R - n_-/\tau_{v1} + n_+e^{-2\beta E_Z^v}/\tau_{v1} \end{cases} \quad (2)$$

where n_{\pm} is the trion population in the K_{\pm} valley, $1/\tau_R$ is the trion recombination rate, and $1/\tau_{v1}$ is the rate for K_- to K_+ intervalley scattering of the trion. In this simple model we have also ignored the possibility that the recombination rate may depend on the valley. The steady state solution is:

$$P_{\text{trion}} = \frac{n_+ - n_-}{n_+ + n_-} = \frac{\frac{\tau_R}{\tau_{v1}} (1 - e^{-2\beta E_Z^v})}{1 + \frac{\tau_R}{\tau_{v1}} (1 + e^{-2\beta E_Z^v})} \approx \frac{\frac{\tau_R}{\tau_{v1}}}{1 + \frac{\tau_R}{\tau_{v1}}} \quad (3)$$

where the second equality is obtained by ignoring the Boltzmann factor $e^{-2\beta E_Z^v} \approx 0.0004$ at 4.2 K and 6.7 T. At low gate voltages we find $P_{\text{trion}} \approx 0.18$ for the data in Fig. 4c of the main text or $\frac{\tau_R}{\tau_{v1}} \approx 0.2$. This is about an order of magnitude larger than the value of $\frac{\tau_R}{\tau_{v1}} \approx 0.03$ found by Ref. [10]; however, their value was obtained in significantly different experimental conditions since they studied WSe_2 samples using resonant excitation and at zero magnetic field. In Fig. 7a, we plot the intervalley scattering rate normalized to the recombination rate $\frac{\tau_R}{\tau_{v1}} \approx |P_{\text{trion}}| / (1 - |P_{\text{trion}}|)$ versus gate voltage. The data shows a linear increase in intervalley scattering with carrier density, consistent with the Bir-Aronov-Pikus mechanism for intervalley hole scattering by the background conduction electrons [2, 11]. As discussed in section 7 of the supplement, we also observe a decrease in the trion polarization with increasing excitation power. This is qualitatively consistent with the rate-equation model assuming that the effective temperature of the trion population increases with excitation power.

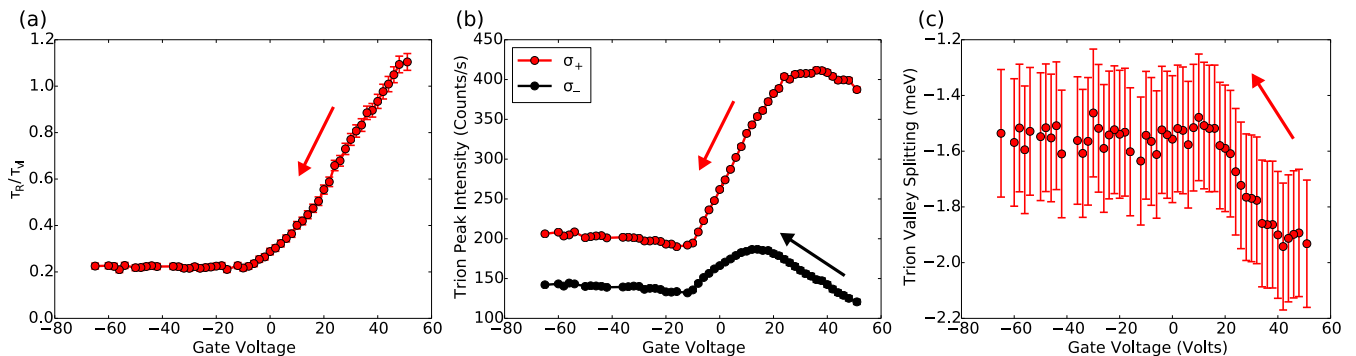


FIG. 7. (a) Gate voltage dependence of $\frac{\tau_R}{\tau_{v1}}$ as defined in the text. This is the same dataset as used for Fig. 4c of the main text: it was taken for sample D2 at 4.2 K and 6.7 T magnetic field, using an excitation power of about $12.5 \mu\text{W}$ and σ_- excitation. The arrow represents the direction of the gate-voltage sweep. (b) Peak intensities of trion luminescence in σ_+ (red) and σ_- (black) detection versus gate voltage at 4.2 K and 6.7 T, taken for sample D2. (c) Trion valley splitting versus gate voltage at 4.2 K and 6.7 T, taken for sample D2.

In Figure 7b we show the peak intensity of trion luminescence in σ_+ and σ_- detection versus gate voltage. At small gate voltages, the trion luminescence intensity increases with increasing gate voltage for both σ_+ and σ_- detection, but the intensity of σ_- luminescence begins to decrease significantly above 15 V. As shown in Fig. 7c, the trion valley splitting changes only for gate voltages above about 15 V, suggesting that the increase in the valley splitting magnitude and decrease in the σ_- intensity could be related. Since the trion can recombine with a range of center of mass wavevectors [12], the change in valley splitting may result from a change in the k -space distribution of the K_- trion population rather than a change in the band Zeeman energies; the trion recombination energy redshifts as

the final state center of mass momentum is increased. The redshift of K_+ trions compared to K_- trions would then correspond to a hot luminescence effect where the trion scattering rate from the K_- to K_+ valley is larger at larger wavevectors.

5. CALCULATIONS OF THE EXCITON VALLEY SPLITTING WITHIN $\mathbf{k} \cdot \mathbf{p}$ THEORY AND TIGHT-BINDING MODELS

The magnetic moment of a band b can be calculated in $\mathbf{k} \cdot \mathbf{p}$ theory using the formula [6, 13–17]:

$$m_b = -\frac{\mu_B}{2m_e} \sum_{a \neq b} \frac{|P_+^{ba}|^2 - |P_-^{ba}|^2}{\epsilon_b - \epsilon_a} \quad (4)$$

where m_e is the free electron mass, μ_B is the Bohr magneton, ϵ_a is the energy of band a , and $P_{\pm}^{ba} = \langle b | p_x \pm ip_y | a \rangle$ is proportional to the optical matrix element for σ_{\pm} light between Bloch states $|a\rangle$ and $|b\rangle$. The formula above gives the z component of the magnetic moment, assuming $\{x, y, z\}$ form a right-handed coordinate system. As discussed in early papers on Bloch electrons in magnetic fields [13, 15], this formula includes both contributions from the phase winding of the Bloch state within a unit cell (the atomic contribution to the magnetic moment) and the phase winding on the scale of multiple unit cells (the intercellular contribution to the magnetic moment). The optical matrix elements are determined by the $\mathbf{k} \cdot \mathbf{p}$ Hamiltonian matrix elements, since $H_{\mathbf{k}, \mathbf{p}} = \frac{\hbar}{2m_e} (k_+ p_- + k_- p_+)$, where $k_{\pm} = k_x \pm ik_y$, $p_{\pm} = p_x \pm ip_y$, and where \mathbf{k} and \mathbf{p} are the wavevector and momentum operator respectively.

In Table V of Ref. [6], Kormányos *et al.* give the non-zero $\mathbf{k} \cdot \mathbf{p}$ matrix elements within their theory. The resulting valley Zeeman energies (as defined in the main text) are:

$$E_Z^c / \mu_B = \frac{2m_e B |\gamma_3 / \hbar|^2}{\epsilon_c - \epsilon_v} - \frac{2m_e B |\gamma_5 / \hbar|^2}{\epsilon_c - \epsilon_{v-3}} - \frac{2m_e B |\gamma_6 / \hbar|^2}{\epsilon_c - \epsilon_{c+2}} \quad (5)$$

in the conduction band and

$$E_Z^v / \mu_B = -\frac{2m_e B |\gamma_3 / \hbar|^2}{\epsilon_v - \epsilon_c} + \frac{2m_e B |\gamma_2 / \hbar|^2}{\epsilon_v - \epsilon_{v-3}} + \frac{2m_e B |\gamma_4 / \hbar|^2}{\epsilon_v - \epsilon_{c+2}} \quad (6)$$

in the valence band, where ϵ_{c+2} is the energy of the second band above the conduction band and ϵ_{v-3} is the energy of the third band below the valence band. Here the parameters γ_i are related to the interband optical matrix elements, and the authors of Ref. [6] determine relevant combinations of these parameters via fits to the DFT band structure [18]. In our case, the precise values of these parameters are not important, as we will focus on the relationship between the effective masses and valley splitting that can be derived using the $\mathbf{k} \cdot \mathbf{p}$ approach. The $\mathbf{k} \cdot \mathbf{p}$ theory effective masses can be written in terms of the γ_i similar to the Zeeman splitting (see Eq. B6 of Ref. [6]). Some simple algebra then allows us to obtain:

$$g_{\text{ex}}^{\text{vl}} = \frac{2(E_Z^c - E_Z^v)}{\mu_B} = 4 - 2 \left(\frac{m_e}{m_c} - \frac{m_e}{|m_v|} \right) \quad (7)$$

where $m_{c(v)}$ is the effective mass of the conduction (valence) band. As long as the effective masses for conduction and valence band are approximately equal, as expected from first principles calculations [18, 19], the valley splitting calculated this way will be close to $g_{\text{ex}}^{\text{vl}} = 4$ and have the opposite sign to our measurements. For example, taking $m_c = 0.49m_e$ and $|m_v| = 0.59m_e$ (these values are from [18]) gives $g_{\text{ex}}^{\text{vl}} = 3.3$.

The exciton valley splitting can also be calculated using a lattice model. For example, Ref. [20] originally proposed a model Hamiltonian for TMDs based on hybridization of d -orbitals at different Mo lattice sites. Such a lattice model neglects the atomic-scale structure of the wave function, and therefore the Zeeman coupling to the d -orbital magnetic moment must be introduced by hand [21, 22]. This gives a contribution to the band Zeeman energies of $E_{Z,a}^c = 0$ and $E_{Z,a}^v = 2\mu_B$, as discussed in the main text. Aside from this contribution, there is the magnetic moment due to phase winding of the Bloch states on the intercellular scale. This quantity can be calculated using the $\mathbf{k} \cdot \mathbf{p}$ theory formula Eq. 4 above, but this time within the reduced Hilbert space of the lattice model. For example, the Hamiltonian in the massive Dirac fermion model is:

$$H = \begin{pmatrix} \epsilon_c & \tau \gamma_3 q_{-\tau} \\ \tau \gamma_3^* q_{\tau} & \epsilon_v \end{pmatrix} \quad (8)$$

written in the basis of band-edge Bloch functions $\{|c\rangle, |v\rangle\}$. The resulting value for the intercellular Zeeman energy is $E_{Z,ic}^{c(v)} = \mu_B \frac{2m_e B |\gamma_3/\hbar|^2}{\epsilon_c - \epsilon_v}$. Here we have used that $\langle c|p_+|v\rangle = 2m_e \gamma_3/\hbar$. We note that $\frac{\hbar^2}{2m_c} = \frac{|\gamma_3|^2}{\epsilon_c - \epsilon_v}$ for this model so that the Zeeman energy is simply $\mu_B B \frac{m_e}{m_c}$. In a given valley this contribution shifts the energy levels in the conduction and valence bands in the same way, and therefore does not contribute to the exciton valley splitting. The total exciton valley splitting for this model is $2(E_Z^c - E_Z^v) = 2(E_{Z,a}^c - E_{Z,a}^v) + 2(E_{Z,ic}^c - E_{Z,ic}^v) = -4\mu_B$ as discussed in the main text. The same approach of separately treating the inter and intra cellular contributions can be used to calculate the exciton valley splitting in more general lattice models where the electron and hole masses are not equal, giving a value for the exciton valley splitting which differs from the bare d -orbital one [21, 22].

Finally, we discuss the effective Hamiltonian for excitons in magnetic field. The exciton Hamiltonian is found by subtracting the conduction and valence band dispersions and adding the electron-hole Coulomb interaction V :

$$H_{\text{ex}} = H_c(-i\hbar\nabla_e, \mathbf{r}_e) - H_v(i\hbar\nabla_h, \mathbf{r}_h) + V(|\mathbf{r}_e - \mathbf{r}_h|) \quad (9)$$

$$= \frac{\hbar^2}{2m_c} (-i\hbar\nabla_e + e\mathbf{A}(\mathbf{r}_e))^2 - \frac{\hbar^2}{2m_v} (-i\hbar\nabla_h - e\mathbf{A}(\mathbf{r}_h))^2 + V(|\mathbf{r}_e - \mathbf{r}_h|) + \frac{1}{2}g_{\text{ex}}^{\text{vl}}\mu_B B\tau. \quad (10)$$

Following Refs. [23, 24], we carry out a gauge transformation to find a one-body Hamiltonian for excitons with zero center of mass momentum:

$$H_{\text{ex}}^\tau = \frac{\hbar^2}{2\mu}\mathbf{k}^2 + \frac{\hbar e B}{2} \left(\frac{1}{m_c} - \frac{1}{|m_v|} \right) l_z + \frac{e^2 B^2}{8\mu} \mathbf{r}^2 + V(|\mathbf{r}|) + \frac{1}{2}g_{\text{ex}}^{\text{vl}}\mu_B B\tau \quad (11)$$

where $\mathbf{r} = \mathbf{r}_e - \mathbf{r}_h$ is the electron-hole separation, \mathbf{p} is the associated canonical momentum, $\mu = m_c|m_v|/(m_c + |m_v|)$, and $l_z = \hat{z} \cdot (\mathbf{r} \times \mathbf{p})$. For bright excitons we assume $l_z = 0$, i.e. that they are s -type [25–27]. Therefore the only term which can give rise to a linear magnetic field dependence of the exciton energy is the last term in Eq. 11, which describes a Zeeman-like coupling of the exciton valley degree of freedom to the magnetic field.

We also estimate the energy shift due to the quadratic term $\frac{e^2 B^2}{8\mu} \mathbf{r}^2$ in the exciton Hamiltonian. In the regime where the magnetic length ($l_B = \sqrt{\frac{\hbar}{eB}}$) is smaller than the exciton Bohr radius, this term leads to a quadratic shift of the exciton transition energy as demonstrated in experiments on quantum wells [24, 28–30]. Theoretically, this could manifest in our experiments as a quadratic term in the valley-averaged transition energy, but due to the small exciton Bohr radius for TMDs (1-3 nm [26, 27]) the correction should be small. We can estimate the diamagnetic shift using perturbation theory with the Wannier model above: the result is a quadratic increase of order $\frac{1}{8}\hbar(\omega_c + \omega_v) \left(\frac{a_B}{l_B} \right)^2 \approx 7 \mu\text{eV}$ at 6.7 T, where $\omega_{c(v)}$ is the electron (hole) cyclotron frequency, and a_B is the exciton Bohr radius. This energy shift is below our measurement sensitivity.

6. EXPERIMENTAL DETERMINATION OF THE SIGN OF THE VALLEY SPLITTING

In the main text, we define the valley splitting as the difference of peak luminescence energies between σ_+ and σ_- polarized emission. Furthermore, σ_\pm polarization is defined as the circular polarization which carries $\pm\hbar$ angular momentum per photon along the field direction for $B > 0$. Equivalently, σ_+ (σ_-) polarized light can be defined as the light with electric field vector rotating counter-clockwise (clockwise) in time around the positive B axis. The convention for $B > 0$ is defined in Fig. 1a of the main text. To determine the sign of the splitting, we used two methods.

First, we determined the rotational settings of the detection polarizer corresponding to different circular polarizations of emission. To do this, we launched circularly-polarized laser light into the cryostat objective lens from the sample space, and found the settings of the detection polarizer which maximized the resulting signal. The circularly-polarized light was generated by sending linearly polarized light through a $\lambda/4$ plate with the light polarized at 45° to the waveplate axes. Given knowledge of the waveplate axes and their orientation relative to the light polarization, the handedness of circularly-polarized light produced in this fashion can be determined. We also checked the assignment of the waveplate fast and slow axes by shining circularly-polarized light of a known handedness through the waveplate and analyzing the resulting linear polarization. For this test, the circularly-polarized light was generated using two N-BK7 prisms in a Fresnel rhomb geometry, so that the resulting handedness could be determined from the Fresnel equations. We determined the field direction using a calibrated Hall probe. The considerations above determine the rotational settings of the detection polarizer corresponding to detection of σ_+ and σ_- emission.

We also compared the valley splitting for MoSe₂ to magnetoluminescence measurements for a (110) cut, undoped, p -type CdTe substrate (from MTI Corporation). For p -type CdTe, the acceptor-bound exciton luminescence shows a

four-fold splitting under magnetic field applied in the Faraday geometry. The optical selection rules lead to circular polarization of these peaks, so that two are σ_+ polarized and two are σ_- polarized. With the detection polarization determined as discussed above, we find peak splitting and selection rules for CdTe in agreement with those found by Refs. [31–33]. In particular, given that the lowest energy acceptor-bound exciton luminescence peak for CdTe is σ_- polarized (for $B > 0$), we know that the lowest energy MoSe₂ peak indeed originates from σ_+ polarized luminescence (for $B > 0$) as indicated in the main text.

7. POWER DEPENDENCE OF TRION POLARIZATION

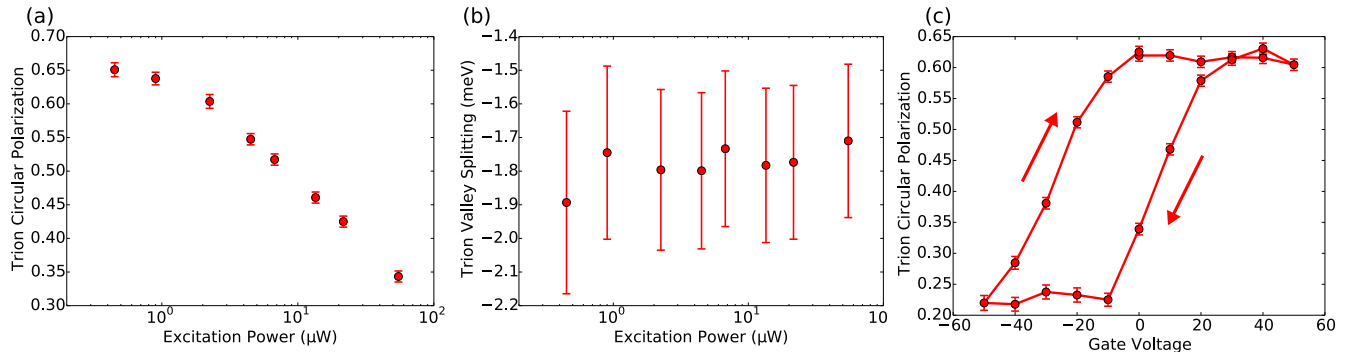


FIG. 8. (a) Trion peak circular polarization versus power in the n -type regime, for $B = 6.7$ T, and excited with σ_- polarized light. (b) Trion valley splitting versus power in the n -type regime and for $B = 6.7$ T. (c) Trion peak circular polarization versus gate voltage, taken at 6.7 T and using about $1.1 \mu\text{W}$ excitation power.

As shown in Fig. 8a, the trion luminescence polarization increases to about 65% circularly-polarized as the power is reduced for $B = 6.7$ T, $T = 4.2$ K, and in the regime of high electron density. On the other hand, we see no power dependence of the trion peak splitting (see Fig. 8b). Within our rate equation model, the power dependence of trion polarization arises from changes in the lattice temperature, or the effective temperature of the trion population which may not be equilibrium with the lattice. A thermometer mounted on the chip holder shows < 50 mK sample heating under more than $200 \mu\text{W}$ excitation, suggesting that the lattice heating is small. Figure 8c shows the gate dependence of trion polarization at 6.7 T and 4.2 K, with an excitation power of about $1.1 \mu\text{W}$; the fractional increase in the trion polarization with gate voltage is similar to data shown in the main text (taken with about $11 \mu\text{W}$ excitation).

-
- [1] G. Kioseoglou, A. T. Hanbicki, M. Currie, A. L. Friedman, D. Gunlycke, and B. T. Jonker, *Appl. Phys. Lett.* **101**, 221907 (2012).
 - [2] K. F. Mak, K. He, J. Shan, and T. F. Heinz, *Nat. Nanotechnol.* **7**, 494 (2012).
 - [3] A. Högele, S. Seidl, M. Kroner, K. Karrai, C. Schulhauser, O. Sqalli, J. Scrimgeour, and R. J. Warburton, *Rev. Sci. Instrum.* **79**, 023709 (2008).
 - [4] J. Ma and Y.-S. Li, *Appl. Opt.* **35**, 2527 (1996).
 - [5] H. Yu, G.-B. Liu, P. Gong, X. Xu, and W. Yao, *Nat. Commun.* **5**, 3876 (2014).
 - [6] A. Kormányos, V. Zólyomi, N. D. Drummond, and G. Burkard, *Phys. Rev. X* **4**, 011034 (2014).
 - [7] G.-B. Liu, W.-Y. Shan, Y. Yao, W. Yao, and D. Xiao, *Phys. Rev. B* **88**, 085433 (2013).
 - [8] K. Kośmider, J. W. González, and J. Fernández-Rossier, *Phys. Rev. B* **88**, 245436 (2013).
 - [9] C. R. L. P. N. Jeukens, P. C. M. Christianen, J. C. Maan, D. R. Yakovlev, W. Ossau, V. P. Kochereshko, T. Wojtowicz, G. Karczewski, and J. Kossut, *Phys. Rev. B* **66**, 235318 (2002).
 - [10] G. Wang, L. Bouet, D. Lagarde, M. Vidal, A. Balocchi, T. Amand, X. Marie, and B. Urbaszek, *Phys. Rev. B* **90**, 075413 (2014).
 - [11] G. L. Bir, A. G. Aronov, and G. E. Pikus, *Zh. Eksp. Teor. Fiz.* **69**, 1382 (1975).
 - [12] J. S. Ross, S. Wu, H. Yu, N. J. Ghimire, A. M. Jones, G. Aivazian, J. Yan, D. G. Mandrus, D. Xiao, W. Yao, and X. Xu, *Nat. Commun.* **4**, 1474 (2013).
 - [13] Y. Yafet, *Solid State Phys* **14**, 1 (1963).
 - [14] W. Yao, D. Xiao, and Q. Niu, *Phys. Rev. B* **77**, 235406 (2008).

- [15] J. M. Luttinger, Phys. Rev. **102**, 1030 (1956).
- [16] L. M. Roth, Phys. Rev. **118**, 1534 (1960).
- [17] S. Wu, J. S. Ross, G.-B. Liu, G. Aivazian, A. Jones, Z. Fei, W. Zhu, D. Xiao, W. Yao, D. Cobden, and X. Xu, Nat. Phys. **9**, 149 (2013).
- [18] A. Kormányos, V. Zólyomi, M. Gmitra, N. D. Drummond, J. Fabian, V. Fal'ko, and G. Burkard, arXiv:1410.6666 (2014).
- [19] A. Ramasubramaniam, Phys. Rev. B **86**, 115409 (2012).
- [20] D. Xiao, G.-B. Liu, W. Feng, X. Xu, and W. Yao, Phys. Rev. Lett. **108**, 196802 (2012).
- [21] A. Srivastava, M. Sidler, A. V. Allain, D. S. Lembke, A. Kis, and A. Imamoglu, arXiv:1407.2624 (2014).
- [22] G. Aivazian, Z. Gong, A. M. Jones, R.-L. Chu, J. Yan, D. G. Mandrus, C. Zhang, D. Cobden, W. Yao, and X. Xu, arXiv:1407.2645 (2014).
- [23] R. S. Knox, *Theory of Excitons* (Academic Press, New York, 1963).
- [24] N. A. Gippius, A. L. Yablonskii, A. B. Dzyubenko, S. G. Tikhodeev, L. V. Kulik, V. D. Kulakovskii, and A. Forchel, J. Appl. Phys. **83**, 5410 (1998).
- [25] G. Berghäuser and E. Malic, Phys. Rev. B **89**, 125309 (2014).
- [26] C. Zhang, H. Wang, W. Chan, C. Manolatou, and F. Rana, Phys. Rev. B **89**, 205436 (2014).
- [27] T. C. Berkelbach, M. S. Hybertsen, and D. R. Reichman, Phys. Rev. B **88**, 045318 (2013).
- [28] M. Sugawara, N. Okazaki, T. Fujii, and S. Yamazaki, Phys. Rev. B **48**, 8848 (1993).
- [29] H. Q. Hou, W. Staguhn, S. Takeyama, N. Miura, Y. Segawa, Y. Aoyagi, and S. Namba, Phys. Rev. B **43**, 4152 (1991).
- [30] D. C. Rogers, J. Singleton, R. J. Nicholas, C. T. Foxon, and K. Woodbridge, Phys. Rev. B **34**, 4002 (1986).
- [31] A. V. Malyavkin, Solid State Commun. **39**, 1315 (1981).
- [32] E. Molva and L. S. Dang, Phys. Rev. B **27**, 6222 (1983).
- [33] E. Molva and L. S. Dang, Phys. Rev. B **32**, 1156 (1985).